Theor Chem Acc (2006) 116: 274–280
DOI 10.1007/s00214-005-0065-1

REGULAR ARTICLE

Pierre-Nicholas Roy

Molecular dynamics with quantum statistics: time correlation functions and weakly bound nano-clusters

Received: 11 April 2005 / Accepted: 26 October 2005 / Published online: 17 December 2005

Abstract An account of recent developments in the study of molecular dynamics with the inclusion of quantum exchange effects is presented. Approaches for quantum dynamical calculations are reviewed and the determination of time correlation functions is a special point of focus. It is shown that the exact basis set techniques can be used to perform highly accurate calculations but are restricted to relatively small systems since computational cost scales exponentially with system size. Alternate formulations can be introduced to circumvent this problem, and semi-classical initial value representation and Feynman path centroid approaches are considered. It is then showed that from a practical point of view, for complex bosonic systems such as doped helium clusters, Quantum Monte Carlo techniques can currently be used for the calculation of quantities of experimental interest. A perspective on future prospects for the calculation of real time correlation functions of bosonic nano-scale systems is presented.

Keywords Quantum Molecular dynamics · Path Integral Monte Carlo · Bose–Einstein centroid dynamics · Semiclassical dynamics

1 Introduction

Time-correlation functions play a central role in statistical mechanics and allow the calculation of transport coefficients, chemical reaction rates and molecular spectra [1–3]. The direct calculation of time correlation functions for quantum mechanical systems is one of the great challenges of theoretical chemistry [4,5]. The task is complicated when one wishes to account for quantum statistical effects present in systems of identical bosons. Various theoretical approaches have been discussed to tackle difficulties with chosen illustrative applications to dope helium clusters.

P.-N. Roy
Department of Chemistry,
University of Alberta,
Edmonton, AB T6G 2G2 Canada
E-mail: pn.roy@ualberta.ca

1.1 Motivation: quantum clusters and droplets

Time-correlation functions are particularly interesting in the context of the dynamics of quantum clusters and droplets since they can be used to explain the behaviour of spectroscopic parameters. A dramatic example is the spectroscopic observation of free molecular rotation in a doped helium nanodroplet and it was proposed that this phenomenon was a microscopic manifestation of superfluidity [6–8]. The effective moment of inertia of the rotating dopant appears to be *renormalized* in these experiments and this, in turn, suggests that part of the helium environment could be dragged by the rotating molecule. The questions raised by these experiments have motivated a growing number of theoretical investigations [9–12]. Note that a quantity that is typically used to characterize rotational spectra is the rotational constant, B, which is inversely proportional to the moment of inertia. Calculations of B have been discussed.

In order to understand the microscopic origins of superfluidity, exciting experimental studies have focused on the size (number N of helium *solvent* atoms) evolution of the spectroscopic properties of doped-helium clusters. A key experimental study was completed for the He_N–OCS system [13]. An important observation of this work was that for cluster sizes ranging from $N = 1 - 8$ the value of the rotational constant, B, undershoots the expected value for a nanodroplet (in the droplet limit, N can be several thousands). With this observation, it was proposed that a mechanism must exists by which the value of the rotational constant increases again. It was suggested that the observation of this 'turnaround' in the rotational constant value versus cluster size could be the sign of the onset of superfluidity. This experiment motivated theoretical studies and Quantum Monte Carlo simulations have been used to explain the turnaround behaviour [14,15]. Such theoretical investigations will be discussed later where time-correlation functions are used to extract spectroscopic parameters.

1.2 Background: time-correlation functions

Before describing the various theoretical approaches, let us first define the correlation function, the main quantity of interest. For a system with Hamiltonian, $\hat{H}$, the canonical real time correlation function for two physical quantities $\hat{A}$ and $\hat{B}$ is defined as,

$$\langle \hat{A}(t)\hat{B}(0)\rangle = \frac{1}{Z}\mathrm{Tr}\left\{ \mathrm{e}^{-\beta\hat{H}}\mathrm{e}^{it\hat{H}/\hbar}\,\hat{A}\,\mathrm{e}^{-it\hat{H}/\hbar}\,\hat{B}\right\}, \qquad (1)$$

where $Z = \mathrm{Tr}\,\mathrm{e}^{-\beta\hat{H}}$ is the partition function and $\beta = 1/k_B T$. Depending on the choice of operators $\hat{A}$ and $\hat{B}$, the above correlation function can be used to obtain transport coefficients or various kinds of spectra. For instance, if operators $\hat{A}$ and $\hat{B}$ are both set to be orientation dipole operators of a rigid linear molecule, the Fourier transform of the correlation function will yield the rotational spectrum. It is in practice very difficult to calculate such real time correlation function directly for complex systems and we present here an account of some of the theoretical approaches that can be used for this purpose. We focus on methods that are currently pratical and also on emerging ideas.

The rest of this article is organized as follows: different approaches for the study of quantum dynamics are first described in general and specific applications of one of the approaches are then presented in the context of doped helium clusters; a conclusion and outlook are finally presented.

2 Approaches for quantum dynamics

Several approaches exist for the treatment of quantum dynamics in molecular systems and we chose to present those that will constitute the tools of choice for the account of both (1) dynamical and (2) quantum exchange effects in doped bosonic clusters. The following discussion is in the context of the Born-Oppenheimer approximation and that the existence of an appropriate potential energy surface (PES) for the system of interest is assumed.

2.1 Exact basis set approaches

In principle, given the Hamiltonian of molecular system, one *simply* needs to select an appropriate set of basis functions, construct the matrix representation of the Hamiltonian, and perform numerical matrix diagonalization in order to obtain the energy levels and wavefunctions. This is, however, only possible for relatively small systems. When the number of degrees of freedom increases, a very attractive alternative to explicit diagonalization is the use of iterative methods such as the Lanczos recursion algorithm [16,17]. This type of approach is very useful in studies of doped helium clusters since exact calculations can be used to assess the quality of model, or ab initio, potential energy surfaces via the comparison between calculated and experimental transition frequencies. A study of this kind was performed for the He–N_2O system [18] where an iterative calculation of the bound states of the complex was performed. This work allowed to establish the quality of a newly proposed PES for He–N_2O.

When two or more identical atoms are present in a floppy weakly bound cluster, the effects of quantum statistics have to be taken into account in order to calculate *physical* eigenstates. For systems of identical atoms obeying Bose–Einstein statistics, the total wavefunction of the system has to be totally symmetric upon the exchange of two (or more) identical bosons. In the context of an iterative method such as the Lanczos approach, it is possible to directly calculate states of a given symmetry using the symmetry-adapted Lanczos (SAL) algorithm [19,20]. This approach has been used to calculate highly accurate excited energy levels of floppy boson trimers of argon and neon [21]. The results of this work have been used as a benchmark in a recent comprehensive study of the neon trimer [22]. The approach of Ref. [21] can also be used to study mixed systems such as small doped helium clusters as in recent work where a cluster composed of two helium atoms and a hydrogen anion was studied [23]. The extension of this work to include a molecular as opposed to an atomic dopant, with two solvating helium atoms, is a current challenge in the field.

We restricted our discussion of exact basis set approaches to *time-independent* techniques where the goal is to obtain energy levels and wavefunctions. With these quantities, it is possible to calculate dynamical properties such as time-correlation functions as discussed later in the context of a comparison to Quantum Monte Carlo methods.

2.2 Semi-classical initial value representation schemes

We briefly mention here a *time-dependent* approach that is approximate in nature but retains many of the essential features of quantum mechanics. The approach is a promising tool for the study of quantum dynamics in doped bosonic clusters but has not yet been used for such problems. It is based on a semi-classical (SC) approximation to the propagator [24] but uses an initial value representation (IVR) that allows the root-search problem of traditional SC techniques to be avoided [25–27]. We refer the reader to a recent review for an account of the topic [28].

Using the popular Herman–Kluk (HK), or coherent state, version of the semiclassical initial value representation (HK-SC-IVR) [29], the propagator, for a system of N particles in three dimensions, can be written as,

$$\mathrm{e}^{-i\hat{H}t/\hbar} = (2\pi\hbar)^{-3N}\int\int \mathrm{d}\mathbf{p}_i\;\mathrm{d}\mathbf{q}_i\, R_{\mathbf{p}_i\mathbf{q}_i t} \times \mathrm{e}^{iS_{\mathbf{p}_i\mathbf{q}_i t}/\hbar}|g_{\mathbf{p}_t\mathbf{q}_t}\rangle\langle g_{\mathbf{p}_i\mathbf{q}_i}|\,, \qquad (2)$$

where $\mathbf{q}_i$ and $\mathbf{p}_i$ are the Cartesian position and momentum vectors, respectively. The subscript i indicates that these correspond to *initial* ($t = 0$) positions and momenta while the subscript t denotes time. The ket $|g_{\mathbf{p}_t\mathbf{q}_t}\rangle$ represents a coherent state at time t [29] and $S_{\mathbf{p}_i\mathbf{q}_i t}$ is the classical action at time t given initial conditions $(\mathbf{p}_i\,,\,\mathbf{q}_i)$. The quantity $R_{\mathbf{p}_i\mathbf{q}_i t}$

is the so-called HK prefactor [29]. This expression for the propagator can then be used to calculate correlation functions such as, for instance, the auto-correlation function of an initial wave-packet $|\phi\rangle$,

$$C(t) = \langle\phi|\mathrm{e}^{-i\hat{H}t/\hbar}|\phi\rangle \ . \tag{3}$$

The Fourier transform of the above correlation function yields the power spectrum,

$$\begin{aligned} I(w) &= \frac{1}{2\pi}\int_{-\infty}^{\infty} \mathrm{d}t\, \mathrm{e}^{i\omega t/\hbar} C(t) \\ &= \sum_n |\langle n|\phi\rangle|^2 \delta(\omega - E_n), \end{aligned} \tag{4}$$

where E_n and $|n\rangle$ are the eigensolutions of the Schrödinger equation, $\hat{H}|n\rangle = E_n|n\rangle$. The "peaks" of the power spectrum, therefore, allow the extraction of the energy levels of a quantum systems. An attractive feature of the SC-IVR is that an approximate quantum mechanical correlation function can be obtained by combining the results of a large number of classical trajectories via Monte Carlo evaluation of the integral appearing in Eq. (2). Several methodological developments of classical molecular dynamics can then be reused in the context of SC dynamics calculations.

In the context of doped bosonic clusters, two essential features have to be considered: (1) the incluson of Bose–Einstein statistics and (2) the treatment of rigid dopants while keeping a simple Cartesian formulation. The inclusion of quantum statistics in SC-IVR methodology has recently been achieved in applications to quantum fluids [30,31]. Methods for the treatment of rigid bonds while maintaining a Cartesian coordinate system have also recently been developed for the HK-SC-IVR [32,33]. A combination of the above two features has not been accomplished to date and would open the door to the direct calculation of real time correlation functions for doped bosonic clusters.

2.3 Bose–Einstein centroid dynamics

Another promising avenue for the calculation of real time correlation functions of complex systems is the use of centroid dynamics methods [34–37]. In these approaches a quantum system is mapped onto a classical-like phase-space that corresponds to the positions and momenta of the centroid (center-of-mass) of Feynman paths [38]. The original formulation of centroid dynamics was derived for Boltzmann statistics and therefore, did not account for exchange effects that are important in our description of doped bosonic clusters. The concepts were extended to the case of Bose–Einstein and Fermi-Dirac statistics [39,40] and the formalism was further developed using path integral techniques [41–43], and an operator formulation [44–47]. An important result of the operator formulation of Bose–Einstein centroid dynamics was the realization that correlation functions involving single particle operators correspond to the double-Kubo transform of regular quantum mechanical correlation functions,

$$\begin{aligned} C(t) &= \frac{1}{\beta^2}\int_0^\beta \mathrm{d}\mu \int_0^\beta \mathrm{d}\nu \left\langle \hat{T}\hat{B}(-i\nu)\hat{A}(t-i\mu)\right\rangle \\ &= \int\int \frac{\mathrm{d}p_c \mathrm{d}q_c}{(2\pi)^{3N}} \frac{\rho_c^{\mathrm{B}}(p_c,q_c)}{Z} \tilde{B}_c \tilde{A}_c(t), \end{aligned} \tag{5}$$

for observables $\hat{A}$ and $\hat{B}$, where $\hat{A}(\tau) = \mathrm{e}^{i\tau\hat{H}}\hat{A}\mathrm{e}^{-i\tau\hat{H}}$, and and $\hat{T}$ is the Dyson time-ordering operator [3]

$$\hat{T}\hat{B}(-i\nu)\hat{A}(t-i\mu) = \begin{cases} \hat{B}(-i\nu)\hat{A}(t-i\mu), & \nu > \mu \\ \hat{A}(t-i\mu)\hat{B}(-i\nu), & \nu < \mu \ . \end{cases} \tag{6}$$

Note that Eq. (5) applies for $\hat{B}$ linear in position and momentum. The second line of Eq. (5) is the centroid correlation function and has a classical-like form. It corresponds to an ensemble average over a centroid phase space, (p_c, q_c). The density function, $\rho_c^{\mathrm{B}}(p_c, q_c)$, is the centroid density, the integral of which yields the exact Bose–Einstein quantum mechanical partition function, Z. The quantities $\tilde{A}_c$ and $\tilde{B}_c$ are the centroid symbols corresponding to operators $\hat{A}$ and $\hat{B}$, respectively, while $\tilde{A}_c(t)$ contains the time-dependence (through equations of motion) of observable A in the centroid representation. Details of the definition of centroid symbols and their equations of motion are given in Ref. [44].

To date, advances in Bose-Einstein centroid dynamics have been formal in nature. Efficient algorithms remain to be developed before these ideas can be applied to doped bosonic clusters and outstanding issues such as the treatment of correlation functions of non-linear operators remain [48]. A relationship between SC and centroid correlation functions has been shown [49] and it will be interesting to establish such a relationship for the Bose–Einstein case. One of the drawbacks of practical centroid dynamics methods is the centroid molecular dynamics (CMD) approximation for which there is no straightforward systematic improvement. Progress has however been made towards increasing the accuracy of CMD through the use of SC-IVR type propagators [50]. Whether one would need to use such techniques to describe the dynamics of doped quantum clusters with centroid dynamics remains an open question.

2.4 Quantum Monte Carlo simulations and connection to experiments

The approaches described above aim at obtaining eigenstates or real-time correlation functions directly. We now describe Quantum Monte Carlo techniques that are applicable to much larger systems but with the difference that correlation functions are calculated in *imaginary* time rather than in real time. Sample results of path integral Monte Carlo (PIMC) simulations for the calculation of imaginary time correlation functions have been chosen to illustrate how imaginary time correlation functions can be used to extract the spectroscopic parameters of doped quantum clusters. These results

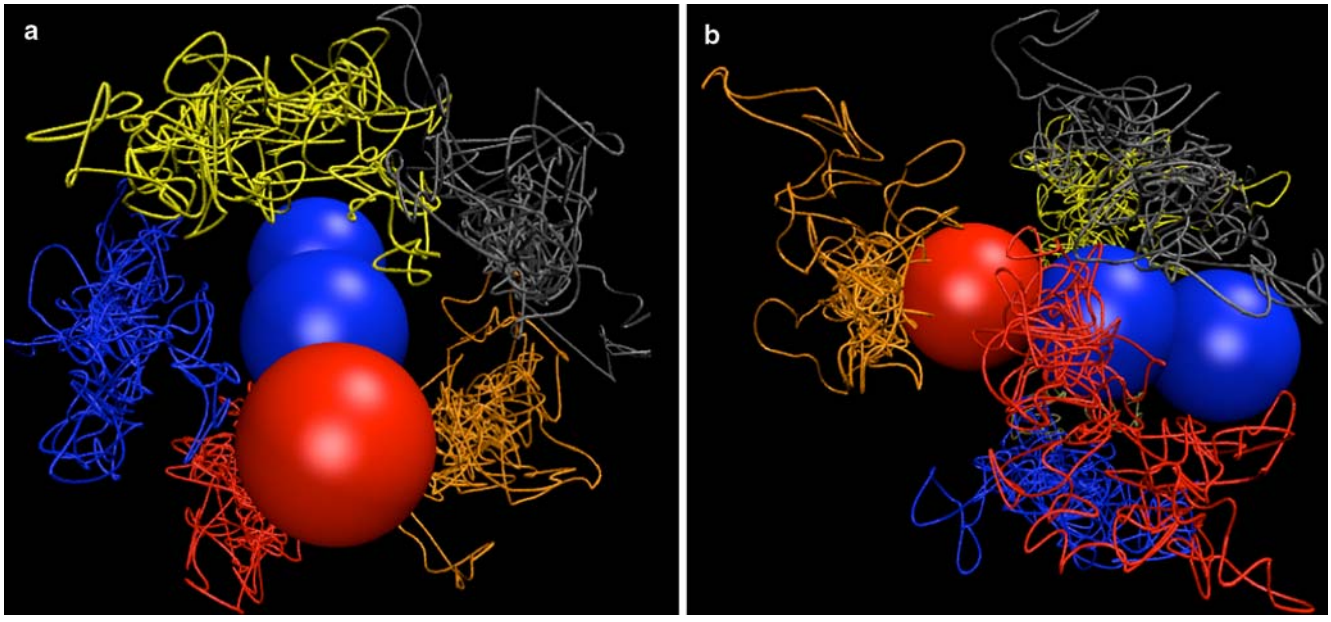

Fig. 1 Feynman Paths for N helium atoms surrounding an N_2O molecular impurity for **a** $N = 5$, and **b** $N = 6$

are based on the simulations presented in Refs. [51] and [52]. We will not describe the approach in details here but will rather report the important aspects pertaining to rotational dynamics. The reader should consult Refs. [51–53] and references therein for details of the PIMC formalism and methodology pertaining to the calculation of rotational correlation functions in doped clusters.

2.4.1 Structural properties

Before presenting calculated correlation functions and their connection to experiments, we illustrate below the Path Integral formalism in the context of a doped helium cluster. In the Path Integral picture, each quantum particle is mapped onto a classical ring polymer, and the quantum statistical properties of the system correspond to the properties of the isomorphic classical polymer system [54] (also see Ref. [55] for a review of PIMC techniques applied to Helium). Properties can be calculated via Monte Carlo integration as a weighted sum over a large number of path (or polymer) configurations.

Helium paths are depicted in Fig. 1 for the He_N–N_2O system. The case of five helium atoms is shown in Fig. 1a. A different colour is assigned to each atom for clarity and the paths a traced in the frame of the N_2O molecular impurity. The paths of the five helium atoms form a ring around the axis of the N_2O molecule. When six helium atoms are present, as shown in Fig. 1b, five helium still form a ring around the molecular axis but the sixth atom goes to the oxygen end of the N_2O molecule. This is due to the nature of the interactions between helium atoms and the N_2O molecule [18].

The paths shown in Fig. 1 are just snapshots of the numerous configurations generated during a Monte Carlo simulation. These configurations can be averaged to obtain the helium density around the N_2O molecule. Such densities have been reported in Ref. [52] as contour plots. We decided to present the same information in Fig. 2 as iso-surfaces in order to provide a three-dimensional perspective. The case of five helium atoms is shown in Fig. 2a where a ring, or donut, arrangement is clearly seen. When the number of helium atoms increases to $N = 8$ as shown in Fig. 2b, a helium cap appears at the oxygen end of the N_2O molecule. The N_2O molecule appears completely surrounded by helium for $N = 10$ as presented in Fig. 2c. It will be shown below that these observations are consistant with experimentally

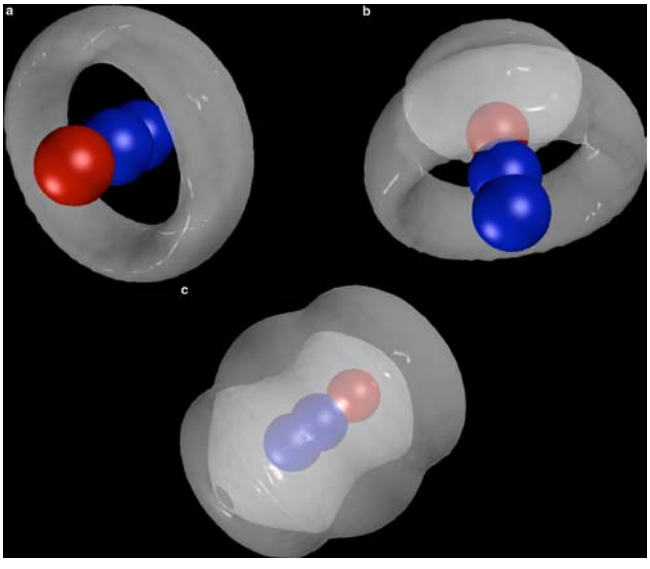

Fig. 2 Helium densities for N helium atoms surrounding an N_2O molecular impurity for **a** $N = 5$, **b** $N = 8$, and **c** $N = 10$

determined structures [56] and can be associated with the rotational dynamics of the doped clusters.

2.4.2 Dynamical properties

Before presenting the analysis of dynamical properties based on imaginary time-correlation functions, we wish to provide an example of a real time correlation function for one helium atom attached to a molecular impurity. Such results are readily obtained from exact basis set calculations of the type presented in the previous section. The quantity of interest is the dipole–dipole correlation function that is obtained from Eq. (1) by replacing the operators $\hat{A}$ and $\hat{B}$ by the unit vector $\mathbf{n}$, which corresponds to the orientation of the molecular impurity with respect to the space-fixed frame. The following quantity is proportional to the dipole–dipole correlation function,

$$\langle \hat{\mathbf{n}}(t) \cdot \hat{\mathbf{n}}(0) \rangle = \frac{1}{Z} \mathrm{Tr} \left\{ \mathrm{e}^{-\beta \hat{H}} \mathrm{e}^{i\hat{H}t/\hbar} \hat{\mathbf{n}} \, \mathrm{e}^{-i\hat{H}t/\hbar} \cdot \hat{\mathbf{n}} \right\}. \quad (7)$$

We show in Fig. 3 the dipole–diople correlation function for the He–OCS complex at a temperature of 0.37 K.

The correlation function, which is composed of contributions from transitions between the eigenstates of the system, clearly contains more than one frequency. This is because at finite temperature, a large number of initial ro-vibrational states of the complex can be populated and transitions to more than one final state can be achieved via dipole coupling. If the real time correlation function is known, the rotational spectrum can be obtained from its Fourier transform in a straightforward way.

Because of the oscillatory nature of the complex trace, the Path Integral Monte Carlo evaluation of real time correlation functions is not practical and we use the imaginary time version instead. In terms of imaginary time, τ, Eq. (7) becomes,

$$\langle \hat{\mathbf{n}}(\tau) \cdot \hat{\mathbf{n}}(0) \rangle = \frac{1}{Z} \mathrm{Tr} \left\{ \mathrm{e}^{-\beta \hat{H}} \mathrm{e}^{\tau \hat{H}} \hat{\mathbf{n}} \, \mathrm{e}^{-\tau \hat{H}} \cdot \hat{\mathbf{n}} \right\}. \quad (8)$$

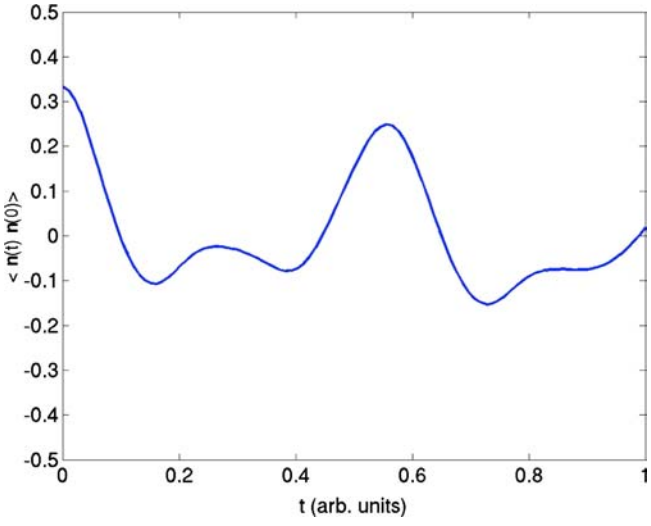

Fig. 3 Real-time orientational correlation function for one helium atom attached to a rigid OCS molecule

This quantity can be calculated for various cluster sizes and is shown in Fig. 4 for the He–OCS dimer. First note how this correlation function differs from its real time counterpart shown in Fig. 3. The signal is now periodic in imaginary time and is composed of a sum of several exponential contributions. The conversion from imaginary to real time of the correlation function involves an inverse Laplace transform and is an ill-posed problem. This means that the rotational spectrum cannot be easily obtained. This dimer calculation was part of the benchmarking of the PIMC approach via a comparison with exact basis set results. The agreement between the basis set and PIMC results was found to be excellent [51]. Another feature of Fig. 4 is the inclusion of the free OCS rotor result for which the correlation function can be calculated analytically. Observe how the free OCS correlation function lies below the He–OCS one. This difference is due to the renormalization of the OCS moment of inertia due to the interaction with the Helium atom. Finally, the fact that the higher temperature correlation function of the dimer lies above the low temperature one is due to the contribution of a larger number of populated excited states.

We saw in Fig. 4 that the moment of inertia of an impurity molecule can be renormalized upon adding a helium atom. As helium atoms are added to the cluster, the moment of inertia will further be modified. Computer simulation studies of He_N–OCS clusters [14,15,51] have been used to provide an explanation for the size dependence of the rotational constant as a function of cluster size. It was shown that if quantum exchange effects were neglected, no turnaround would be observed in the size dependence of the rotational constant [51]. In this work, in order to circumvent the inverse Laplace transform difficulties, the rotational constants were extracted from the correlation functions by fitting them to a free rotor model. Another approach that could have been used is the analytic continution of the imaginary time-correlation function using maximum entropy methods [57]. Such techniques have been used in the past to analyse PIMC data for various properties [58–63].

A study on He_N–$\mathrm{N_2O}$ clusters allowed the first experimental observation of a turnaround in the size dependence of the rotational constant [56]. These experimental results are presented Fig. 5 along with two types of simulation results. It is clear from the figure that at around $N = 8$, there is a turnaround in the behaviour of the experimental rotational constant that is indicative of some decoupling mechanism. Following this experimental work, a theoretical study was completed in order to resolve some outstanding questions. It was, for instance, proposed that the turnaround in the behaviour of the rotational constant was due to exchange effects [56]. By combining ground state Quantum Monte Carlo and Boltzmann PIMC calculations, it was possible to directly establish that exchange effects were indeed responsible for the turnaround [52]. The simulation results are both shown in Fig. 5. The ground state results agree very well with experiment for all cluster sizes while the Boltzmann PIMC results (where exchange is neglected) start departing from the experimental ones at cluster sizes greater than 8, the point of the

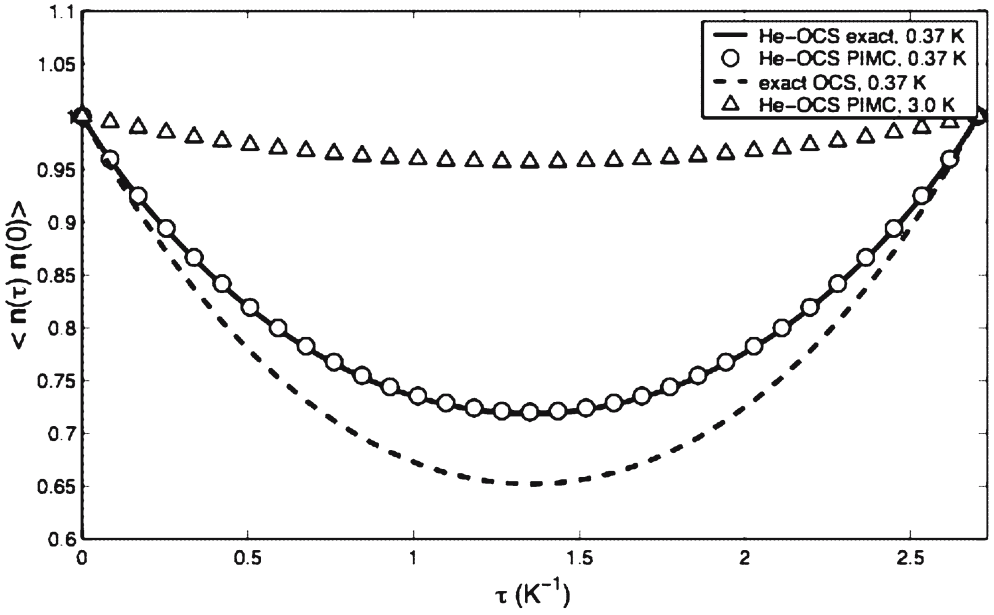

Fig. 4 Imaginary time-correlation function for one helium atom attached to a rigid OCS molecule. PIMC (*circles*) and exact (*solid line*) results are presented along with the exact free rotor correlation function (*dashed line*) for a temperature of 0.37 K. PIMC results (*triangles*) are also presented for a temperature of 3.0 K. The imaginary time axis of the 3.0 K results has been scaled to make the correlation function comparable to the 0.37 K ones

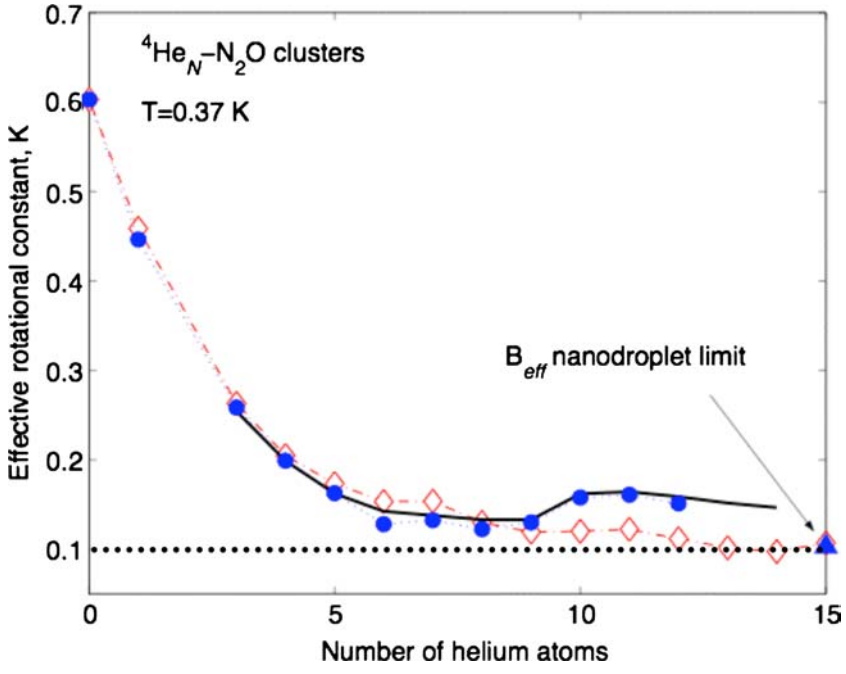

Fig. 5 Evolution of the rotational constant B as function of cluster size N. Boltzmann PIMC (*diamonds*), ground state (*solid line*) and experimetal (*filled circles*) results are presented. The nanodroplet limit is indicated by a *dotted line* and a *filled triangle*

turnaround. It can then be suggested that exchange effects are essential in order to capture the turnaround and decoupling. By inspecting the isosurfaces presented earlier in Fig. 2, one can see that for $N = 10$, where the decoupling is strong, the dopant molecule is completely surrounded by helium atoms. Such an arrangement favours exchanges between the helium atoms.

In a very recent work, the first comparison of the effects of Bose–Einstein and Boltzmann statistics on the size dependence of the moment of inertia of rotating doped helium clusters was achieved [53]. The approach was applied to CO_2 doped helium clusters and it was shown that exchange effects were important to explain the qualitative decoupling behaviour of the experimental spectrum. The methods described

earlier are currently being used to investigate other systems in a joint theory-experiment effort to provide a unified picture for the behaviour of doped quantum clusters.

3 Conclusion and outlook

A brief account of the methods geared towards the calculation of the dynamical properties of doped bosonic clusters has been presented. We remarked that exact basis set methods are restricted to systems of smaller sizes but can nevertheless be quite useful in benchmarking alternate schemes designed to tackle bigger problems. It is clear that at present, the Quantum Monte Carlo family of methods is the path of choice for the study of the experimentally observed size dependence of the spectroscopic signatures of doped bosonic clusters. For the calculation of spectra, the technique is not without problems as one has to rely on imaginary time-correlation functions. The present discussion was restricted to correlation functions and the question of the estimation of superfluidity in rotating clusters was omitted. This topic is discussed in Ref. [53]. An ultimate goal in the field of quantum clusters is to charter the molecular origins of superfludity in finite size systems and truly bridge the gap between the cluster and nanodroplet size regimes.

Finally, in the context of doped bosonic quantum clusters, SC-IVR and Bose–Einstein centroid formulations are emerging techniques with the promise of yielding real time correlation functions directly. These two areas are very exciting avenues for future investigations.

Acknowledgements The author thanks Nicholas Blinov, Wolfgang Jäger and Yunjie Xu for stimulating discussions. This work was supported by the Natural Sciences and Engineering Research Council of Canada, the Canada Foundation for Innovation, and The Research Corporation.

References

1. Zwanzig R (1965) Annu Rev Phys Chem 16: 67
2. Chandler DG (1987) Introduction to modern statistical mechanics. Oxford University Press, New York
3. Kubo R, Toda M, Hashitsume N (1991) Statistical physics. II Nonequilibrium statistical mechanics. Springer, Berlin Heidelberg New York
4. Thirumalai D, Berne BJ (1983) J Chem Phys 79: 5029
5. Thirumalai D, Berne BJ (1984) J Chem Phys 81: 2512
6. Grebenev S, Toennies JP, Vilesov AF (1998) Science 279: 2083
7. Toennies JP, Vilesov AF (1998) Annu Rev Phys Chem 49: 1
8. Lehmann KK, Scoles G (1998) Science 279: 2065
9. Whaley KB (1998) Adv Mol Vib Collision Dyn 3: 397
10. Callegari et al C (1999) Phys Rev Lett 83: 5058
11. Kwon Y, Huang P, Patel MV, Blume D, Whaley KB (2000) J Chem Phys 113: 6469
12. Draeger E, Ceperley D (2003) Phys Rev Lett 90: 065301
13. Tang J, Xu Y, McKellar ARW, Jäger W (2002) Science 297: 2030
14. Moroni S, Sarsa A, Fantoni S, Schmidt KE, Baroni S (2003) Phys Rev Lett 90: 143401
15. Paesani F, Viel A, Gianturco FA, Whaley KB (2003) Phys Rev Lett 90: 073401
16. Cullum JK, Willoughby RA (1985) Lanczos algorithms for large symmetric eigenvalue computations. Birkhäuser, Boston
17. Carrington T Jr (1998) von Ragué Schleyer P (ed) Encyclopedia of computational chemistry, vol 5. Wiley, New York
18. Song X, Xu Y, Roy P-N, Jager W (2004) J Chem Phys 121: 12308
19. Wang X-G, Carrington T Jr (2001) J Chem Phys 114: 1473
20. Chen R, Guo H (2001) J Chem Phys 114: 1467
21. Roy P-N (2003) J Chem Phys 119: 5437
22. Baccarelli I et al (2005) J Chem Phys 122: 084313
23. Liu Y, Roy P-N (2004) J Chem Phys 121: 6282
24. Vleck V (1928) Proc Natl Acad Sci USA 14: 178
25. Miller WH (1970) J Chem Phys 53: 3578
26. Miller WH (1991) J Chem Phys 95: 9428
27. Heller E (1991) J Chem Phys 94: 2723
28. Thoss M, Wang H (2004) Annu Rev Phys Chem 55: 299
29. Herman M, Kluk E (1984) Chem Phys 91: 27
30. Nakayama A, Makri N (2004) Chem Phys 304: 147
31. Nakayama A, Makri N (2005) Proc Natl Accad Sci 102: 4230
32. Harland BB, Roy P-N (2003) J Chem Phys 118: 4791
33. Issack BB, Roy P-N (2005) J Chem Phys 123: 084103
34. Cao J, Voth GA (1994) J Chem Phys 100: 5106
35. Voth GA (1996) Adv Chem Phys XCIII: 135
36. Jang S, Voth GA (1999) J Chem Phys 111: 2357
37. Jang S, Voth GA (1999) J Chem Phys 111: 2371
38. Feynman RP, Hibbs AR (1965) Quantum mechanics and path integrals. McGraw-Hill, New York
39. Roy P-N, Voth GA (1999) J Chem Phys 110: 3647
40. Roy P-N, Jang S, Voth GA (1999) J Chem Phys 111: 5303
41. Kinugawa K, Nagao H, Ohta K (1999) Chem Phys Lett 307: 187
42. Blinov NV, Roy P-N, Voth GA (2001) J Chem Phys 115: 4484
43. Kinugawa K, Nagao H, Ohta K (2001) J Chem Phys 114: 1454
44. Blinov NV, Roy P-N (2001) J Chem Phys 115: 7822
45. Blinov NV, Roy P-N (2002) J Chem Phys 116: 4808
46. Roy P-N, Blinov NV (2002) Isr J Chem 42: 183
47. Moffatt P, Blinov N, Roy P-N (2004) J Chem Phys 120: 4614
48. Reichman DR, Roy P-N, Jang S, Voth GA (2000) J Chem Phys 113: 919
49. Shi Q, Geva E (2003) J Chem Phys 118: 8173
50. Ka BJ, Voth GA (2004) J Phys Chem B 108: 6883
51. Blinov N, Song X, Roy P-N (2004) J Chem Phys 120: 5916
52. Moroni S, Blinov N, Roy P-N (2004) J Chem Phys 121: 3577
53. Blinov N, Roy P-N (2005) J Low Temp Phys 140: 253
54. Chandler D, Wolynes PG (1981) J Chem Phys 74: 4078
55. Ceperley DM (1995) Rev Mod Phys 67: 279
56. Xu Y, Jäger W, Tang J, McKellar ARW (2003) Phys Rev Lett 91: 163401
57. Skilling J, (ed) (1989) Maximum entropy and Bayesian methods. Kluwer, Cambridge, UK
58. Gallicchio E, Berne B (1994) J Chem Phys 101: 9909
59. Jarrell M, Gubernatis J (1996) Phys Rep 269: 134
60. Boninsegni M, Ceperley D (1996) J Low Temp Phys 104: 339
61. Kim D, Doll J, Gubernatis JE (1997) J Chem Phys 106: 1641
62. Krilov G, Sim E, Berne B (2001) Chem Phys 268: 21
63. Rabani E, Reichman DR, Krilov G, Berne BJ (2002) Proc Natl Acad Sci USA 99: 1129